Journal of Renewable Materials

Tech Science Press

DOI: 10.32604/jrm.2023.025011

check for updates

ARTICLE

Investigation of the Nd-Ce-Mg-Zn/Substituted Hydroxyapatite Effect on Biological Properties and Osteosarcoma Cells

Suha Q. AL-Shahrabalee* **and Hussein Alaa Jaber**

Department of Materials Engineering, Baghdad, 10001, Iraq

*Corresponding Author: Suha Q. AL-Shahrabalee. Email: mae.19.09@grad.uotechnology.edu.iq

Received: 17 June 2022 Accepted: 02 August 2022

ABSTRACT

Cancerous diseases and diseases resulting from bacteria and fungi are some of the pressures that humans face. Therefore, the development of biomaterials that are resistant to cancerous diseases, bacteria, and fungi has become one of the requirements of the medical field to extend the life of the biomaterial and fight pathogens after implanting these materials inside the human body. One of the important biomaterials used in the field of orthopedics is hydroxyapatite. In this research, Nano substituted hydroxyapatite was prepared by the wet precipitation method, including replacing 5% of the calcium ions with neodymium, cerium, magnesium, and zinc ions in cationic substitution. Many tests were carried out to characterize the prepared material. The biological properties were evaluated by examining the resistance of the substituted hydroxyapatite to bacteria and fungi, in addition to testing the effect of the material on normal cells and bone cancer cells. The results showed a new structure of hydroxyapatite after the substitution process and a significant improvement in the biological properties of the prepared biomaterial compared to other researches.

KEYWORDS

Hydroxyapatite; neodymium; cerium; substitution

Nomenclature

λ	Wave length of CuKα radiation
θ	Theta (angle of Bragg)
β	Full width at half maximum (FWHM)
ACP	Amorphous Calcium Phosphate
MTT	3-(4,5-dimethylthiazol-2-yl)-2,5-diphenyl-2H-tetrazolium bromide
WRL68	The human hepatic cell line
MG63	Osteosarcomas
μm	Micrometer
SD	Standard Deviation

1 Introduction

Hydroxyapatite (HA), a common substance in the orthopedic and orthodontic sectors, exhibits good biocompatibility [1], cellular function promotion, bioactivity, and osteoconductivity. This inorganic

phosphate has gained significant attention for medical applications in the form of powders, composites, and coatings due to its chemical and structural resemblance with the mineral phase of bone and teeth [2–4]. Despite the aforementioned characteristics, synthetic HA has limited use as a bone graft material due to several problems, including achieving the optimum crystallinity level, phase purity, low mechanical properties, and high *in vitro* solubility [5,6]. To solve these problems, extensive research is being conducted to produce HA metal composite or ion substituted/HA using various techniques [7–9]. Ionic substitution has emerged as a powerful technique for enhancing the performance of HA, either by modifying its structural, morphological, and chemical characteristics or by leveraging the substituting ions' therapeutic effects [10,11]. Stoichiometric HA has a unit cell that hosts ten cationic organized in two non-equivalent positions [12], which is what permits the apatite structure to be stable and flexible, allowing for a variety of cationic and anionic substitutions such as (Sr^{2+}, Mg^{2+}, Zn^{2+}) or/and (SiO_4^{4-}, F^-, CO_3^{2-}), respectively. Despite the scope of these isomorphous substitutions being slight, they critically regulate many of the HA properties like biological activity, the interaction between these biomaterial and bone minerals by inducing dissolution rate, crystal growth, solubility, drug delivery efficiency, morphology, surface chemistry, and the mechanical properties [13,14].

In comparison to pure HA, neodymium substituted hydroxyapatite (Nd/HA) with various doping levels exhibited a considerable increase in electrical conductivity, which is essential in the electromagnetic sector and for the accelerating of bone fracture repair. The biocompatibility test of the Nd/HA NPs on the L929 fibroblast cell line revealed that cell viability was greater than 90%, with no effect on cell proliferation. Nd/HA can deliver anticancer medications with high specificity while also allowing for fluorescence imaging, which would be a significant advancement in cancer therapy [15]. Another therapeutic ion that is gaining popularity in biological applications is cerium (Ce) [16]. Cerium is indeed a rare-earth metal that does not accumulate in the food chain and it is renowned for its cholesterol-lowering, blood-pressure-lowering, and blood-clot-prevention characteristics in humans [17]. It has been shown to promote osteoblast proliferation, increase bone mechanical qualities, induce bone formation, and have antimicrobial effects [18]. It has the ability to mimic enzymes such as superoxide dismutase, catalase, and oxidase, all of which have biological benefits like antioxidant capabilities. In physiological fluids, cerium can also change its oxidation states (Ce^{3+} and Ce^{4+}), reducing reactive oxygen species in order to maintain good biological functioning [19]. Magnesium and zinc are important elements needed by the human body, Mg is an important trace element in human bones and is one of the elements that can use as a cationic substitute for Ca in the HA lattice. Above everything else, having the right ratio of Mg to Ca is essential for preventing and curing osteoporosis. Mg is known to boost osteoblast-like cell proliferation, calcification, and angiogenic activities, as well as promote cellular adherence to the substrate. As a result, adding Mg to synthetic HA is critical for a variety of reasons, including increased bioactivity [20]. Zinc ions are an important trace element for tissue regeneration and have antimicrobial characteristics, but they also operate as crystal growth inhibitors. Zn/HA stimulates osteoblast proliferation and differentiation, potentially improving osteointegration in the field of biomaterials and for future applications in orthopedics and dental implants [21].

The wet chemical precipitation method was used to produce (Nd-Ce-Mg-Zn) substituted hydroxyapatite nanoparticles in this investigation. X-ray diffraction (XRD), Fourier-transform infrared spectroscopy (FT-IR), Field Emission Scanning Electron Microscope (FE-SEM) and energy dispersive spectroscopy (EDS) with mapping were used to examine the influence of Nd, Ce, Mg, and Zn insertion on the structural and biological characteristics of the resulting substituted hydroxyapatite. Antibacterial and antifungal activity, as well as investigate the effect of substituted HA on normal cells (WRL68) and osteosarcoma cells (MG63).

2 Materials and Method

2.1 Synthesis of Substituted Hydroxyapatite

Chemical precipitation is regarded as a method of hydroxyapatite production that requires the use of aqueous solutions in which chemical reactions between calcium and phosphorus ions occur at a controlled pH and temperature. According to theoretical calculations, the molar ratio (Ca + Nd + Ce + Mg + Zn/P) for the substituted hydroxyapatite was equal to 1.67 according to the following equation:

$$\frac{Ca + Nd + Ce + Mg + Zn}{P} = \frac{0.063 + 0.00095 + 0.00095 + 0.00095 + 0.00095 + 0.00095}{0.039997} = 1.67$$

where 5% of the calcium ions were replaced with substituted ions by 1.25% for each substituted ion and the preparation was according to the following steps:

1. An aqueous solution of the total nitrate salts (0.167 M) was prepared by mixing calcium nitrate tetrahydrate (14.986 g), neodymium nitrate hexahydrate (0.366 g), cerium nitrate hexahydrate (0.363 g), magnesium nitrate hexahydrate (0.214 g), and zinc nitrate hexahydrate (0.248 g) with deionized water (400 mL) at room temperature and at a speed of 300 rpm, where this solution is regarded the source of calcium ions and substituted ions.
2. The sources of phosphorous ions were obtained by preparing 0.1 M of $(NH_3)_2HPO_4$ (5.282 g with 400 mL of deionized water) and using ammonia to raise the basicity of the phosphorous ion solution to above 10.5, then this solution was drop-wise in the nitrate salts solution at controlled pH and temperature (70°C).
3. After complete dropping, the pH was adjusted to 11 gradually and the heating was stopped to allow the solution aging for one day (24 h) with a continuous stirrer at room temperature.
4. The neutralization reaction is the most prevalent reaction that results in the production of water as a byproduct which was removed by filtration and the filtered powder was washed many times with deionized water, dried at 100°C for about 8 h, sintered at 800°C for 2 h at a heating rate of 5 °C/min, and grind to obtain Nano Nd-Ce-Mg-Zn/HA as indicated in Fig. 1.

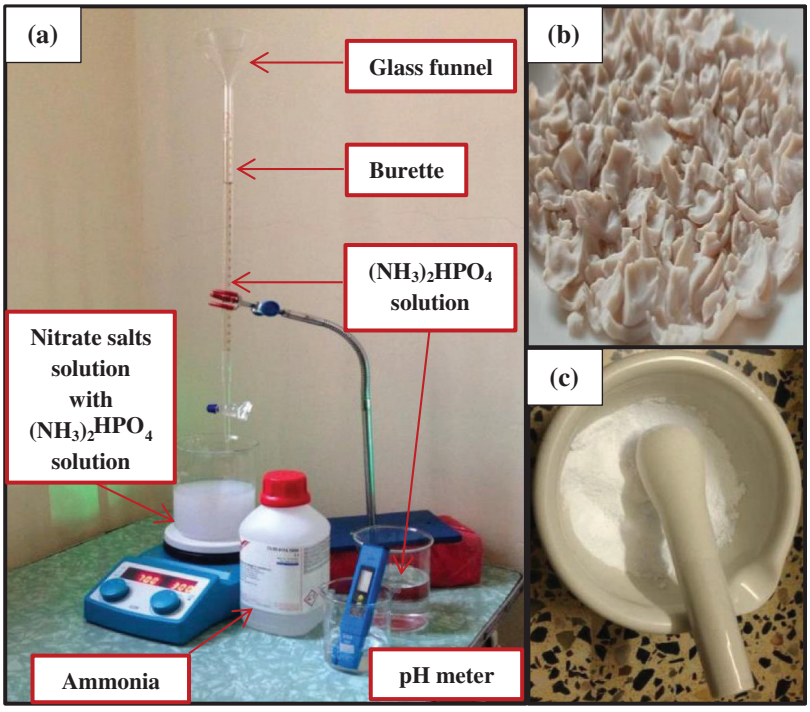

Figure 1: Preparation method steps of substituted HA (a) Chemical reactions, (b) Flake of Nd-Ce-Mg-Zn/HA, and (c) Grind the flake manually

2.2 Substituted HA Characterization Tests

2.2.1 XRD Test

XRD technique was applied to verify the formation of substituted HA and their constituent in the specimens under study (Philips X'Pert X-ray PRO, Holland) operating with CuKα radiation (λ = 1.5405 Å) was used to obtain the X-ray diffraction for Nd-Ce-Mg-Zn/HA after completing the preparation steps of substituted HA using the wet precipitation method. The data was drawn with a step of 0.05° point/second in 2θ between 10° and 80°. Besides that, phases were identified by comparing the peak positions of the experimental XRD patterns with those of the X'Pert HighScore Plus.

2.2.2 Fourier Transform Infrared Spectroscopy Test (FTIR)

FTIR spectroscopy was used to characterize the functional groups of Nd-Ce-Mg-Zn/HA utilizing a Bruker Tensor 27 IR, Germany, where the spectral range was from 4000 to 500 cm^{-1} by using potassium bromide pellets (KBr). When the transmittance mode is used, the acquired FTIR spectra will represent the entire material.

2.2.3 Field Emission Scanning Electron Microscope (FE-SEM) with Energy Dispersive Spectroscopy (EDS)

A Field Emission Scanning Electron Microscope (FE-SEM) was used to characterize the morphology and size of the sample; moreover, an Energy Dispersive Spectroscopy (EDS) measurement was obtained in the same equipment to confirm the existence of Ca, Nd, Ce, Mg, Zn, P, and O in the prepared substituted HA and help in the calculation of the new Ca + M/P ratio. All verification tests were taken using (Zeiss Sigma 300-HV, Germany).

2.3 Biological Examinations

2.3.1 Antimicrobial Activity of Nd-Ce-Mg-Zn/HA

One of the most important characteristics of hydroxyapatite is its antibacterial and antifungal activity. The activity of synthesized HA was tested against three types of gram-positive bacteria *(Staphylococcus aureus*, *Staphylococcus epidermidis*, and *Streptococcus mutans*) and one type of gram-negative bacteria (*Escherichia coli*). The activity of substituted HA was also tested against fungi, with *Candida albicans* as the chosen fungus. The activation of microorganisms was performed in the laboratory under controlled conditions, and biological activity was measured using the wells diffusion method. For antibacterial activity, gentamicin tablets with a concentration of 10 micrograms were used as a comparison, while for fungal activity, nystatin was used.

2.3.2 Cytotoxicity Assay

The effect of produced material on normal cell lines, as well as the anticancer activity of Nd-Ce-Mg-Zn/HA, was investigated using an MTT assay on the WRL68 and MG63 cell lines. The cells were cultured and incubated (in a CO_2 incubator at 37°C). Serial dilutions were prepared for substituted HA (from 6.25 to 400 μg/mL). Each concentration of substituted HA was added to MG63 cells, and these cultured cells were incubated at 37°C in the presence of 5% CO_2 for enough time. MTT solution (10 μL) was added to these wells and again incubated with 5% CO_2 at 37°C. The media was removed and a solubilization solution was added to each well to solubilize the formazan crystals. After complete incubation in a humidified atmosphere, the specimens' absorbance was measured by the use of an ELISA reader (Bio-rad, Germany) at 575 nm. A statistical analysis (Graph Pad Prism) was utilized to finalize the results.

3 Results of Characterization and Biological Tests

3.1 XRD

Fig. 2 depicts the sintered HA's XRD pattern. The pattern shows the typical peaks of HA at 26.0540°, 28.2663°, 31.8628°, 34.2336°, 39.9905°, 42.2488°, 43.9810°, 46.8897°, 49.6631°, 53.3685°, 64.2619°, 71.9393°, and 77.1786° according to JCPDS cards number (00-001-1008) and (96-900-1234). As for the

4 substitution elements, it was found that peaks 28.2663°, 29.1634°, 31.8628°, 34.2336°, 42.2488°, 49.6631°, 61.8490°, 71.9393°, and 77.1786° correspond the JCPDS cards number (00-039-0914), (00-052-0798), and (01-089-2922) which belongs to neodymium element, while the peaks 28.2663°, 29.1634°, 31.8628°, 33.1325°, 34.2336°, 39.9905°, 49.6631°, 56.0836°, 61.8490°, 64.2619°, 71.9393°, and 77.1786° belongs to cerium element according to JCPDS cards number (00-033-0324), (00-038-0762), and (01-089-2728); regarding magnesium, the peaks 31.8628°, 34.2336°, and 77.1786° matches the JCPDS cards number (00-001-1141) and (00-004-0770); finally, 77.1786° peak was found that it matched the data in JCPDS card number of zinc (98-065-3502). In comparison with normal hydroxyapatite prepared by the same method, it was found that the main peaks of normal HA are situated at 25.88°, 31.78°, 32.20°, 32.93°, 34.06°, 39.82°, 46.69°, 49.48°, and 52.08°, also, the d spacing was 3.43, 2.81, 2.77, 2.71, 2.63, 2.26, 1.94, 1.84, and 1.75 Å, respectively [22].

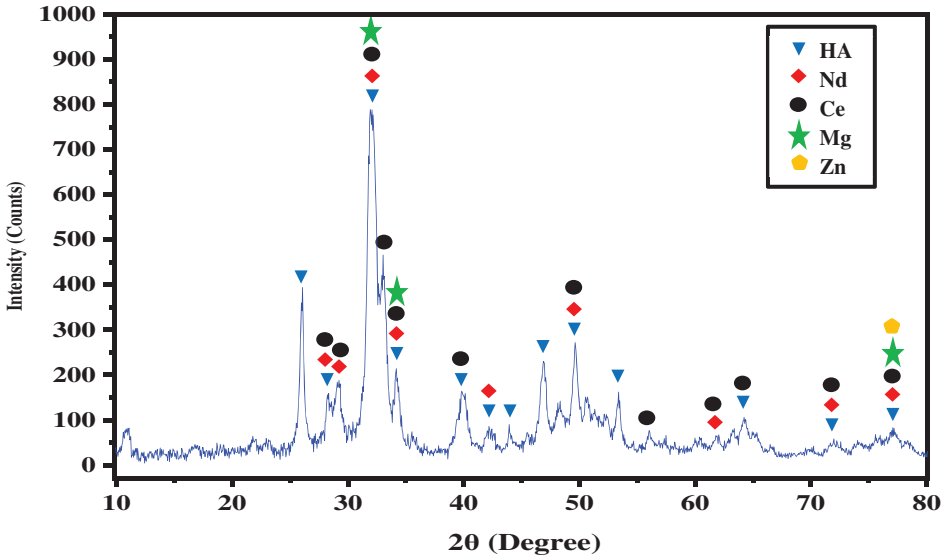

Figure 2: XRD test to investigate the formation of substituted HA with its substituted elements

The hydroxyapatite crystal system is hexagonal [23] and the lattice parameters were determined through certain mathematical calculations involving the use of d-spacing and Miller indices (Table 1), it was found that the value of these constants after substitution part of calcium ions with neodymium, cerium, magnesium, and zinc are 9.387 Å for a and b while the value of the lattice constant c was 6.8669 Å. The average crystal size of Nd-Ce-Mg-Zn/HA is 28.3 nm and it was calculated by using Debye-Scherrer's equation:

$$d = K\lambda/\beta \cos\theta$$

where K is the constant of shape, λ is the X-ray beam wave length, β is FWHM of the peak, and θ is the angle of Bragg [24].

Table 1: Data extracted from the XRD test of Nd-Ce-Mg-Zn/HA

Peak position 2θ (°)	FWHM	Interplaner spacing d (Å)	Miller indices (hkl)
26.0540	0.2952	3.42015	002
28.2663	0.2952	3.1573	012
31.8628	0.3444	2.80865	121
34.2336	0.3936	2.61938	022

(Continued)

Table 1 (continued)

Peak position 2θ (°)	FWHM	Interplaner spacing d (Å)	Miller indices (hkl)
39.9905	0.5904	2.25458	310
42.2488	0.7872	2.13915	032
43.9810	0.2952	2.05884	113
46.8897	0.3444	1.93768	222
49.6631	0.2952	1.83578	123
53.3685	0.2952	1.71673	004
64.2619	0.3936	1.44952	233
71.9393	0.984	1.31255	044
77.1786	0.96	1.23498	153

3.2 FTIR Test

The synthetic substituted HA infrared spectra are shown in Fig. 3 which explain all the functional groups in Nd-Ce-Mg-Zn/HA structure. The hydroxyl (OH^-) vibrational groups can be recognized in bands at 629.36 and 3571.43 cm^{-1} in these spectra which regard as one of the essential chemical groups in HA. Bands related to phosphate groups (PO_4^{3-}) were also discovered at a wavenumber of 963.17, 1021.39, and 1088.15 cm^{-1} where stoichiometric hydroxyapatite has this functional group. Due to the conditions of preparation, many chemical groups were noticed in addition to these two essential groups (PO_4^{3-}, OH^-) and Table 2 includes a list of the wavenumbers for the additional functional groups of Nd-Ce-Mg-Zn/HA.

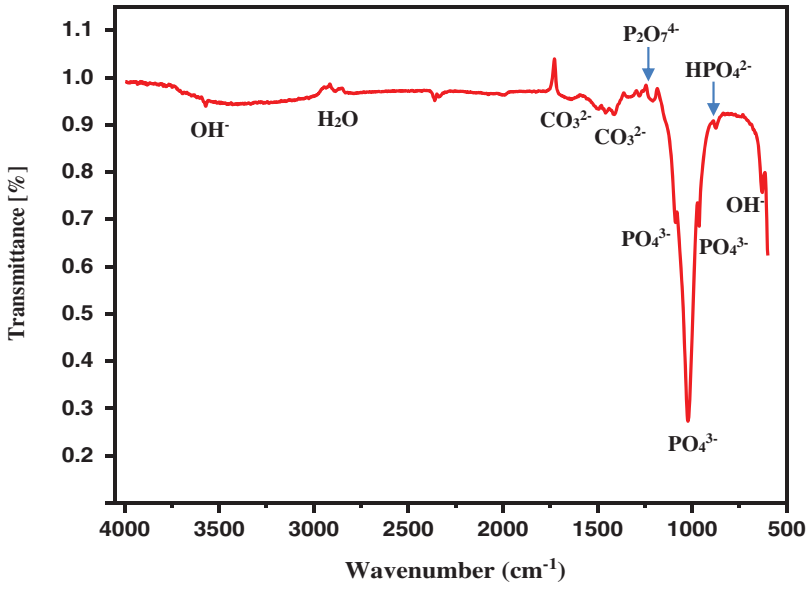

Figure 3: FTIR spectroscopy of Nd-Ce-Mg-Zn/HA with the explanation of functional groups

Table 2: Chemical groups of Nd-Ce-Mg-Zn/HA with its description

Chemical groups	Wavenumber (cm^{-1})	Description	Reference
$(OH)^{-}$	629.36	Prove formation of HA	[25]
	3571.43		[26]
$(HPO_4)^{3-}$	874.19	Characterizes HA with calcium deficient	[27]
$(PO_4)^{3-}$	963.17	Prove formation of HA	[28]
	1021.39		[29]
	1088.15		[30]
$(P_2O_7)^{4-}$	1208.14	Originates when $1.5 < Ca/P < 1.677$	[27]
$(CO_3)^{2-}$	1342.18	The low intensity of CO_3^{2-} indicates a greater assay degree	[29]
	1411.65		[31]
	1457.28		[29]
	1493.77		[32]
H_2O	2885.32	The absorption band narrows as a result of the thermal treatment	[33]

3.3 FE-SEM and EDS

The analysis by FE-SEM at a magnification of 60.00 and 5.00 KX with the resolution of 200 nm and 2 μm, respectively exhibited the formation of nano-sized cluster-like particles for Nd-Ce-Mg-Zn/HA powder prepared by the wet precipitation method. The Posner cluster could potentially represent one of those clusters as indicated in Fig. 4. The ACP particle sizes are affected by the pH of the solution, the concentrations of the mixing reagents, and the preparation temperature; for instance, a higher supersaturation yields smaller ACP particles [34].

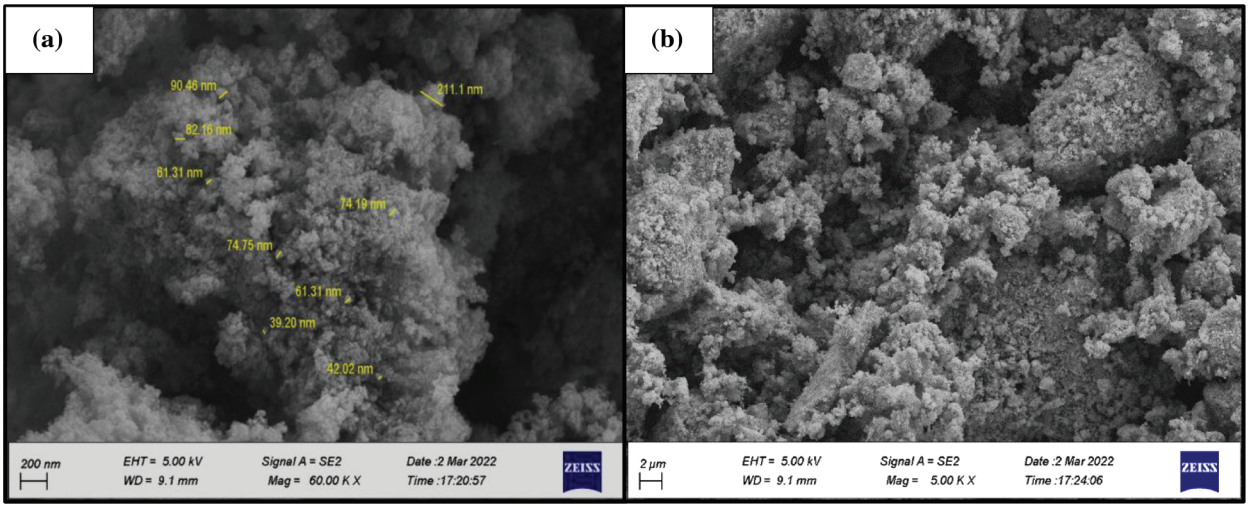

Figure 4: FE-SEM of (a) particle size of Nd-Ce-Mg-Zn/HA and (b) Nd-Ce-Mg-Zn/HA

The chemical composition of substituted hydroxyapatite was explained in Fig. 5 where the EDS test shows the presence of essential elements of hydroxyapatite with substituted elements. From the attached table, it is obvious that the Ca/P ratio will change after substitution to Ca + Nd + Ce + Mg + Zn/P and become equal to 1.66 which is very close to the bone molar ratio (1.67). The two key factors that affect the Ca/P ratio are the change in pH and sintering temperature [35] where substituted HA was prepared at a pH of 11 and the sintering process was the step that followed the preparation process at a temperature of 800°C. Thus, the theoretical calculations of the molar ratio will be very close to the practical results if the basic factors of the reaction are controlled correctly.

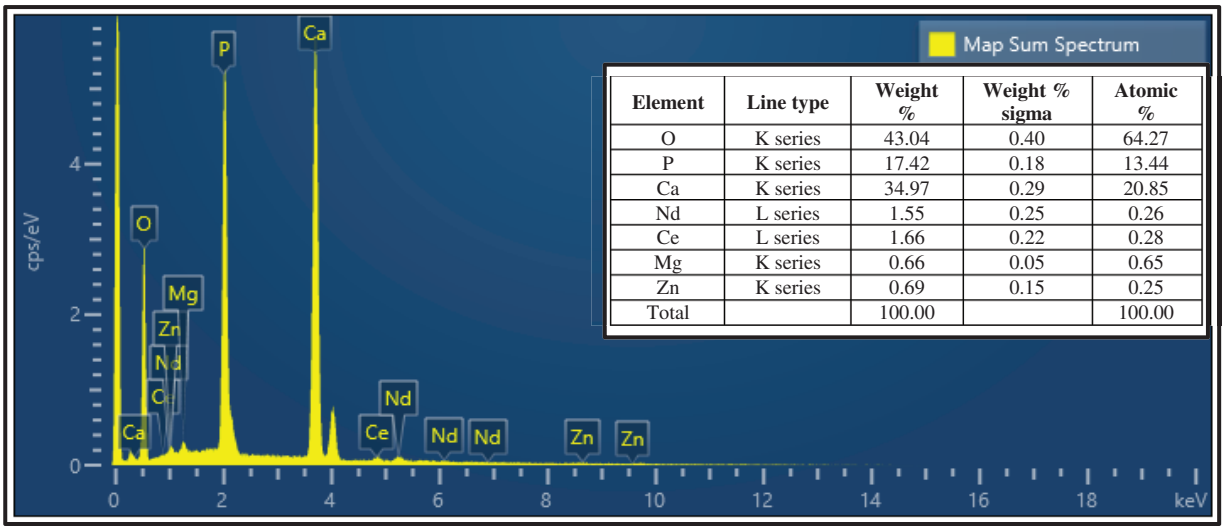

Element	Line type	Weight %	Weight % sigma	Atomic %
O	K series	43.04	0.40	64.27
P	K series	17.42	0.18	13.44
Ca	K series	34.97	0.29	20.85
Nd	L series	1.55	0.25	0.26
Ce	L series	1.66	0.22	0.28
Mg	K series	0.66	0.05	0.65
Zn	K series	0.69	0.15	0.25
Total		100.00		100.00

Figure 5: EDS analysis of Nd-Ce-Mg-Zn/HA

It is necessary to show the distribution of essential and substituted elements that compose substituted HA and this was obvious in Fig. 6.

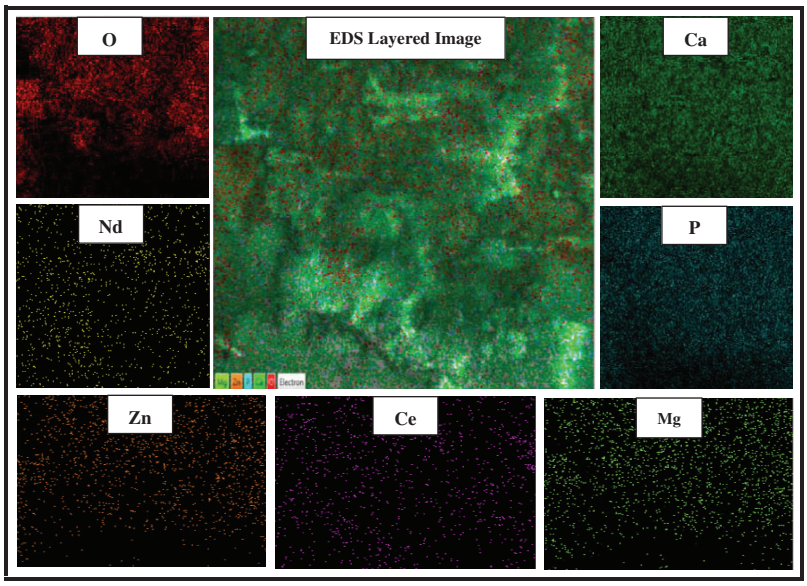

Figure 6: EDS mapping to explain Nd-Ce-Mg-Zn/HA elemental distribution at 2 μm resolution

3.4 Antibacterial and Fungicide Activity

Many bacterial species have developed antibiotic resistance, prompting efforts to develop novel materials with effective antibacterial capabilities. It is also worth noting that bacterial adherence and biofilm formation induce implant-related bone infections. As a result, it appears that seeking new antibacterial techniques is justified. Substituted HA is one of the active biomaterials for intraoperative treatment and prevention of bone infections where nanometer-sized HA can efficiently decrease antibacterial activity when doped or cationic-substituted [36]. It is evident from Fig. 7 that Nd-Ce-Mg-Zn/HA is highly resistant to bacteria and fungi as compared to gentamicin and nystatin, respectively.

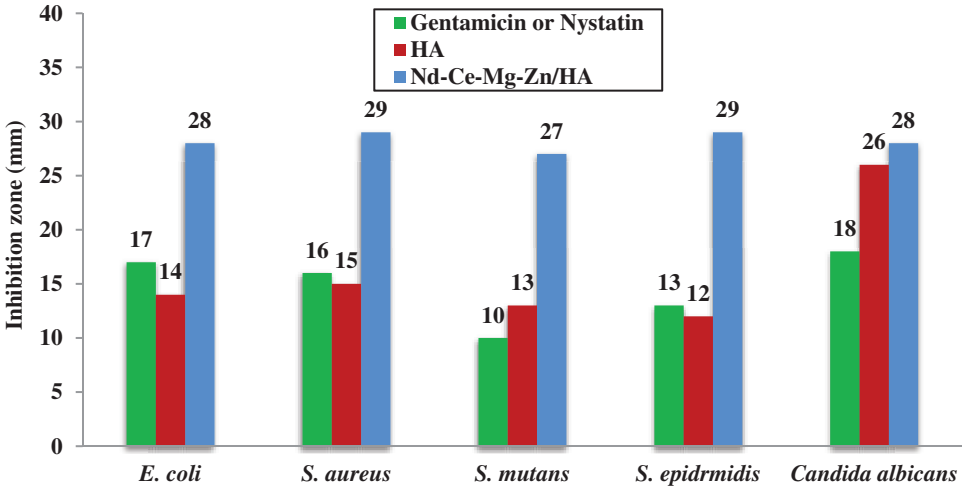

Figure 7: Antibacterial and fungicide activity of Nd-Ce-Mg-Zn/HA

3.5 MTT Assay

It is obvious from the relationship between viability and concentration in Fig. 8 that Nd-Ce-Mg-Zn/HA has a high value of IC_{50} for both the normal cell line (265.2 μg/mL) and the cancer cell line (206.1 μg/mL). The dose-dependent pattern of Nd-Ce-Mg-Zn/HA (Table 3) had the highest value of the reduction in osteosarcoma cells (37.81 ± 2.38)% compared to (25.73 ± 4.34)% for normal cells at the concentration of 400 μg/mL whereas, the effect of substituted HA on MG63 at low concentrations had nearly consistent viability of (94.83 ± 0.71)%, (94.87 ± 0.29)%, (95.95 ± 0.90)%, and (94.29 ± 0.82)% at 6.25, 12.5, 25, and 50 μg/mL, respectively. However, at 400 μg/mL, it increased to (62.19 ± 2.38)%, indicating that Nd-Ce-Mg-Zn/HA had significant anticancer activity ($P < 0.0001$) against the MG63 cell line at high concentrations while the effect of the prepared substituted HA remains somewhat safe on normal cells (WRL68).

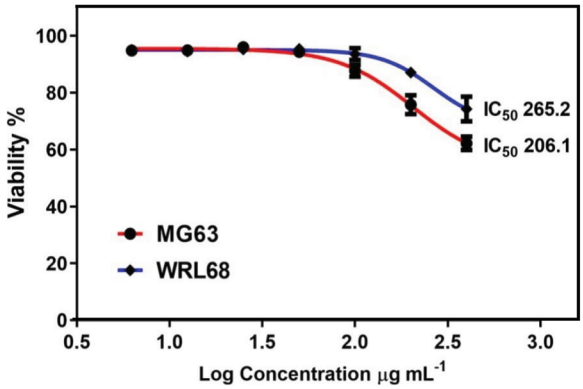

Figure 8: Relationship between viability and Log concentration to explain the cytotoxic effect of Nd-Ce-Mg-Zn/HA on MG63 and WRL68 cell lines

Table 3: Cytotoxicity effect of Nd-Ce-Mg-Zn/HA on MG63 and WRL68 cell lines

Concentration (μg/mL)	Viability %			
	MG63		WRL68	
	Mean ± SD	Specimens number	Mean ± SD	Specimens number
400	62.19 ± 2.38	3	74.27 ± 4.34	3
200	75.81 ± 3.33	3	87.11 ± 1.46	3
100	87.73 ± 2.09	3	93.60 ± 2.10	3
50	94.29 ± 0.82	3	95.33 ± 1.18	3
25	95.95 ± 0.90	3	95.22 ± 0.82	3
12.50	94.87 ± 0.29	3	94.48 ± 1.55	3
6.25	94.83 ± 0.71	3	95.02 ± 0.83	3

4 Discussion

The inclusion of new elements in hydroxyapatite leads to the formation of new biomaterials with a new structure and biological properties. So, the first step after the synthesis process is making characterize test to ensure the formation of substituted HA. The first test was XRD which revealed the formation of HA with the existence of substitution elements. XRD test followed by FTIR spectroscopy revealed the presence of many functional groups in addition to the essential HA groups ($(PO_4)^{3-}$, OH^-), this is due to the fact that synthetic HA is made by reacting two solutions in an aqueous environment, which promotes the synthesis of a large number of functional groups in the structure of prepared substituted HA, the most important of which is the presence of carbonate groups. The bioactivity of HA powder will improve because the negative charge carriers initiate and encourage the development of bone-type apatite in the existence of the SBF [37].

FE-SEM test showed the formation of Posner clusters which are ACP structural units with a globular-like structure that have been postulated as mineralization precursors. They have a size in the nanometer range. Also, there are a lot of globular-like particles that do not seem to be nodular-type defects but could be ACP cluster agglomerates [38]. ACP is a mineral phase that forms in mineralized tissues and was the first manufactured industrial hydroxyapatite where before that it had previously been found in the otoliths of blue sharks, as well as in chiton teeth as a precursor phase of carbonated hydroxyapatite [39]. ACP is thought to have a unique role as a precursor to bioapatite and as a transient stage in biomineralization [40]. Elements of rare earth including Nd and Ce are regarded as toxic to bacteria and fungi. In the existence of rare earth elements, many filamentous fungi hyphae have abnormal morphological features. Multiple terminal branching, lateral branching, swelling, and the breaking of hyphal strands by a mechanism analogous to plasmolysis are among these changes. Asexual spore formation is likewise inhibited by these elements [41]. Mg/HA has antibacterial activity against both gram-positive and gram-negative bacteria as well as is efficient against the development of the *C. albicans* fungi cell [42]. The main mechanisms involved in the antimicrobial activities of Mg-based materials have indeed been described as being identical to those seen in other metallic ions. As a result, the literature demonstrated that nanoparticles are often toxic to organisms by causing oxidative stress, inflammation, or even indirect or direct DNA damage, as well as by producing species of reactive oxygen, which cause oxidative DNA damage, lipid peroxidation, and protein denaturation [43]. Regarding Zn, it was found that Zn/HA has active resistance against common human pathogens from bacteria and fungi including *S. aureus, E. coli* [44], *S. mutans*, and *C. albicance* [45]. There are various facets to the mechanism by which zinc ions inhibit microbial growth where zinc ions harm the cell membranes and increase cell permeability.

Furthermore, Zn interacts with the proper functioning of bacterial enzymes (like ATPase, pyruvate kinase, or glycolytic enzymes) [46]. Thus, these four substitution elements in HA structure act in a professional way to resist bacteria and fungi compared with the normal HA, where the antimicrobial effect of HA is much lower than the prepared substituted HA [47].

Nd-doped hydroxyapatite is regarded as safe for humans at a different rate of Ca substitution including 1%, 5%, 10%, and 20% [48]; in addition to that, it can deliver anticancer medications with high specificity while also allowing for fluorescence imaging, which would be a significant advancement in cancer therapy [49]. The MTT assay of Ce doped HA shows good biocompatibility at specific concentrations, and *in vitro*, it displays cytocompatibility with MG63 osteoblasts at dosages of 200–600 μg/mL [15]. Regarding magnesium and zinc, it is known that both are essential elements needed by the human body and they have high biocompatibility with alive cells, where they maintained the survival and spread of endothelial and osteoblast (OBs) cells, enhanced OBs adhesion and boosted cell proliferation. On the other hand, they have cytocompatibility with many cancer cells such as MC3T3-E1 and MG63 [50]. From this, it is clear that the addition of neodymium, cerium, magnesium, and zinc to the structure of HA makes their work synergistically to improve bone properties and resist bacteria, fungi, and cancer cells.

5 Conclusion

Hydroxyapatite seems to be a key component in bioceramics and is extensively utilized in dental implantology and reconstruction medicine. Despite the scaffold for newly created bone, we may see a tendency to widen the spectrum of apatite materials with additional biological, physicochemical, or biomechanical capabilities. It is necessary to investigate the potential of ions with antibacterial properties being substituted. Substituted hydroxyapatite has been prepared by the wet precipitation method and its characterization tests were done by using several analytical tools such as XRD, FTIR, and SEM-EDS techniques. These tests indicate the formation of hydroxyapatite with its functional groups and the existence of the substitute elements (Nd, Ce, Mg, and Zn) in the new structure of HA, which led to a significant change in the biological properties. As the presence of these elements led to an increase in the resistance of hydroxyapatite to many types of bacteria and fungi, in addition, it is safe on normal cells (WRL68) and it has an anticancer effect on MG63.

Acknowledgement: The authors are grateful to The University of Technology in Baghdad and The Faculty of Medicine (FOM)/The University of Malaya in Kuala Lumpur.

Funding Statement: The authors received no specific funding for this study.

Conflicts of Interest: The authors declare that they have no conflicts of interest to report regarding the present study.

References

1. Anaee, R. A. (2016). Behavior of Ti/HA in saliva at different temperatures as restorative materials. *Journal of Bio- and Tribo-Corrosion, 2(2),* 1–9. DOI 10.1007/s40735-016-0036-1.
2. Castro, M. A. M., Oliveira, T. P., Correia, G. S., Oliveira, M. M., Rangel, J. H. G. et al. (2020). Synthesis of hydroxyapatite by hydrothermal and microwave irradiation methods from biogenic calcium source varying PH and synthesis time. *Boletín de la Sociedad Española de Cerámica y Vidrio, 61(1),* 35–41. DOI 10.1016/j.bsecv.2020.06.003.
3. Anwar, A., Akbar, S., Sadiqa, A., Kazmi, M. (2016). Novel continuous flow synthesis, characterization and antibacterial studies of nanoscale zinc substituted hydroxyapatite bioceramics. *Inorganica Chimica Acta, 453,* 16–22. DOI 10.1016/j.ica.2016.07.041.

4. Balu, S., Sundaradoss, M. V., Andra, S., Jeevanandam, J. (2020). Facile biogenic fabrication of hydroxyapatite nanorods using cuttlefish bone and their bactericidal and biocompatibility study. *Beilstein Journal of Nanotechnology, 11(1),* 285–295. DOI 10.3762/bjnano.11.21.
5. Bigi, A., Boanini, E., Capuccini, C., Gazzano, M. (2007). Strontium-substituted hydroxyapatite nanocrystals. *Inorganica Chimica Acta, 360(3),* 1009–1016. DOI 10.1016/j.ica.2006.07.074.
6. Boanini, E., Gazzano, M., Bigi, A. (2010). Ionic substitutions in calcium phosphates synthesized at low temperature. *Acta Biomaterialia, 6(6),* 1882–1894. DOI 10.1016/j.actbio.2009.12.041.
7. Bollino, F., Armenia, E., Tranquillo, E. (2017). Zirconia/hydroxyapatite composites synthesized via sol-gel: Influence of hydroxyapatite content and heating on their biological properties. *Materials, 10(7),* 757. DOI 10.3390/ma10070757.
8. Destainville, A., Champion, E., Bernache-Assollant, D., Laborde, E. (2003). Synthesis, characterization and thermal behavior of apatitic tricalcium phosphate. *Materials Chemistry and Physics, 80(1),* 269–277. DOI 10.1016/S0254-0584(02)00466-2.
9. Dhafer, G., Al-Shroofy, M. N., Al-Kaisy, H. A. (2022). Electrostatic deposition of bio-composite polymer/hydroxyapatite coatings on 316L stainless steel. *Key Engineering Materials, 911,* 40–45. DOI 10.4028/p-40btz7.
10. Donadel, K., Felisberto, M. D. V., Laranjeira, M. C. M. (2009). Preparation and characterization of hydroxyapatite-coated iron oxide particles by spray-drying technique. *Anais da Academia Brasileira de Ciencias, 81(2),* 179–186. DOI 10.1590/S0001-37652009000200004.
11. Dorozhkin, S. V. (2012). Amorphous calcium orthophosphates: Nature, chemistry and biomedical applications. *International Journal of Materials and Chemistry, 2(1),* 19–46. DOI 10.5923/j.ijmc.20120201.04.
12. Eanes, E. D. (1998). Amorphous calcium phosphate: Thermodynamic and kinetic considerations. In: *Calcium phosphates in biological and industrial systems*, pp. 21–39. USA: Springer. DOI 10.1007/978-1-4615-5517-9_2.
13. Farid, S. B. H. (2018). Bioceramics: For materials science and engineering. In: *Bioceramics: For materials science and engineering*. UK: Woodhead Publishing. DOI 10.1016/C2016-0-04604-1.
14. Ferraris, S., Yamaguchi, S., Barbani, N., Cazzola, M., Cristallini, C. et al. (2020). Bioactive materials: *In vitro* investigation of different mechanisms of hydroxyapatite precipitation. *Acta Biomaterialia, 102,* 468–480. DOI 10.1016/j.actbio.2019.11.024.
15. Gheisari, H., Karamian, E., Abdellahi, M. (2015). A novel hydroxyapatite–hardystonite nanocomposite ceramic. *Ceramics International, 41(4),* 5967–5975. DOI 10.1016/j.ceramint.2015.01.033.
16. Hargreaves, J. S. J. (2016). Some considerations related to the use of the scherrer equation in powder X-ray diffraction as applied to heterogeneous catalysts. *Catalysis, Structure and Reactivity, 2(1–4),* 33–37. DOI 10.1080/2055074X.2016.1252548.
17. Hong, Z., Zhang, P., He, C., Qiu, X., Liu, A. et al. (2005). Nano-composite of poly(L-lactide) and surface grafted hydroxyapatite: Mechanical properties and biocompatibility. *Biomaterials, 26(32),* 6296–6304. DOI 10.1016/j.biomaterials.2005.04.018.
18. Iconaru, S. L., Predoi, M. V., Chapon, P., Gaiaschi, S., Rokosz, K. et al. (2021). Investigation of spin coating cerium-doped hydroxyapatite thin films with antifungal properties. *Coatings, 11(4),* 464. DOI 10.3390/coatings11040464.
19. Ito, A., Kawamura, H., Miyakawa, S., Layrolle, P., Aomori, R. et al. (2001). Resorbability reduction by the incorporation of zinc into tricalcium phosphate. *Key Engineering Materials, 192–195,* 199–202. DOI 10.4028/www.scientific.net/kem.192-195.199.
20. Kaygili, O., Keser, S., Dorozhkin, S. V., Yakuphanoglu, F., Al-Ghamdi, A. A. et al. (2014). Structural and dielectrical properties of Ag- and Ba-substituted hydroxyapatites. *Journal of Inorganic and Organometallic Polymers and Materials, 24(6),* 1001–1008. DOI 10.1007/s10904-014-0074-4.
21. Kokubo, T., Kim, H. M., Kawashita, M. (2003). Novel bioactive materials with different mechanical properties. *Biomaterials, 24(13),* 2161–2175. DOI 10.1016/S0142-9612(03)00044-9.
22. Kumar, G. S., Girija, E. K., Venkatesh, M., Karunakaran, G., Kolesnikov, E. et al. (2017). One step method to synthesize flower-like hydroxyapatite architecture using mussel shell bio-waste as a calcium source. *Ceramics International, 43(3),* 3457–3461. DOI 10.1016/j.ceramint.2016.11.163.

23. Kurtuldu, F., Mutlu, N., Michálek, M., Zheng, K., Masar, M. et al. (2021). Cerium and gallium containing mesoporous bioactive glass nanoparticles for bone regeneration: Bioactivity, biocompatibility and antibacterial activity. *Materials Science and Engineering: C, 124,* 112050. DOI 10.1016/j.msec.2021.112050.
24. Leung, Y. H., Ng, A. M. C., Xu, X., Shen, Z., Gethings, L. A. et al. (2014). Mechanisms of antibacterial activity of Mgo: Non-ros mediated toxicity of Mgo nanoparticles towards Escherichia coli. *Small, 10(6),* 1171–1183. DOI 10.1002/smll.201302434.
25. Li, Y., Ooi, C. P., Cheang Hong Ning, P., Aik Khor, K. (2009). Synthesis and characterization of neodymium (III) and gadolinium (III)-substituted hydroxyapatite as biomaterials. *International Journal of Applied Ceramic Technology, 6(4),* 501–512. DOI 10.1111/j.1744-7402.2008.02293.x.
26. De Lima, I. R., Alves, G. G., Soriano, C. A., Campaneli, A. P., Gasparoto, T. H. et al. (2011). Understanding the impact of divalent cation substitution on hydroxyapatite: An *in vitro* multiparametric study on biocompatibility. *Journal of Biomedical Materials Research–Part A, 98(3),* 351–358. DOI 10.1002/jbm.a.33126.
27. Meejoo, S., Maneeprakorn, W., Winotai, P. (2006). Phase and thermal stability of nanocrystalline hydroxyapatite prepared via microwave heating. *Thermochimica Acta, 447(1),* 115–120. DOI 10.1016/j.tca.2006.04.013.
28. Nicolini, V., Malavasi, G., Menabue, L., Lusvardi, G., Benedetti, F. et al. (2017). Cerium-doped bioactive 45S5 glasses: Spectroscopic, redox, bioactivity and biocatalytic properties. *Journal of Materials Science, 52(15),* 8845–8857. DOI 10.1007/s10853-017-0867-2.
29. Odusote, J. K., Danyuo, Y., Baruwa, A. D., Azeez, A. A. (2019). Synthesis and characterization of hydroxyapatite from bovine bone for production of dental implants. *Journal of Applied Biomaterials & Functional Materials, 17(2)*. DOI 10.1177/2280800019836829.
30. Panda, S., Biswas, C. K., Paul, S. (2021). A comprehensive review on the preparation and application of calcium hydroxyapatite: A special focus on atomic doping methods for bone tissue engineering. *Ceramics International, 47(20),* 28122–28144. DOI 10.1016/j.ceramint.2021.07.100.
31. Pietak, A. M., Reid, J. W., Stott, M. J., Sayer, M. (2007). Silicon substitution in the calcium phosphate bioceramics. *Biomaterials, 28(28),* 4023–4032. DOI 10.1016/j.biomaterials.2007.05.003.
32. Predoi, D., Iconaru, S. L., Deniaud, A., Chevallet, M., Michaud-Soret, I. et al. (2017). Textural, structural and biological evaluation of hydroxyapatite doped with zinc at low concentrations. *Materials, 10(3),* 229. DOI 10.3390/ma10030229.
33. Predoi, D., Iconaru, S. L., Predoi, M. V., Motelica-Heino, M., Buton, N. et al. (2020). Obtaining and characterizing thin layers of magnesium doped hydroxyapatite by dip coating procedure. *Coatings, 10(6),* 510. DOI 10.3390/COATINGS10060510.
34. Prosolov, K. A., Belyavskaya, O. A., Rau, J. V., Prymak, O., Epple, M. et al. (2018). Deposition of polycrystalline zinc substituted hydroxyapatite coatings with a columnar structure by RF magnetron sputtering: Role of in-situ substrate heating. *Journal of Physics: Conference Series, 1115(3),* 032077. DOI 10.1088/1742-6596/1115/3/032077.
35. Prosolov, K. A., Lastovka, V. V., Belyavskaya, O. A., Lychagin, D. V., Schmidt, J. et al. (2020). Tailoring the surface morphology and the crystallinity state of Cu- and Zn-substituted hydroxyapatites on Ti and Mg-based alloys. *Materials, 13(19),* 4449. DOI 10.3390/ma13194449.
36. Rodríguez-Lugo, V., Karthik, T. V. K., Mendoza-Anaya, D., Rubio-Rosas, E., Villaseñor Cerón, L. S. et al. (2018). Wet chemical synthesis of nanocrystalline hydroxyapatite flakes: Effect of PH and sintering temperature on structural and morphological properties. *Royal Society Open Science, 5(8),* 180962. DOI 10.1098/rsos.180962.
37. Sheikh, L., Sinha, S., Singhababu, Y. N., Verma, V., Tripathy, S. et al. (2018). Traversing the profile of biomimetically nanoengineered iron substituted hydroxyapatite: Synthesis, characterization, property evaluation, and drug release modeling. *RSC Advances, 8(35),* 19389–19401. DOI 10.1039/c8ra01539b.
38. Skwarek, E., Janusz, W., Sternik, D. (2017). The influence of the hydroxyapatite synthesis method on the electrochemical, surface and adsorption properties of hydroxyapatite. *Adsorption Science & Technology, 35(5–6),* 507–518. DOI 10.1177/0263617417698966.

39. Stipniece, L., Stepanova, V., Narkevica, I., Salma-Ancane, K., Boyd, A. R. (2018). Comparative study of surface properties of Mg-substituted hydroxyapatite bioceramic microspheres. *Journal of the European Ceramic Society, 38(2),* 761–768. DOI 10.1016/j.jeurceramsoc.2017.09.026.
40. Talburt, D. E., Johnson, G. T. (1967). Some effects of rare earth elements and yttrium on microbial growth. *Mycologia, 59(3),* 492–503. DOI 10.2307/3756768.
41. Tank, K. P., Chudasama, K. S., Thaker, V. S., Joshi, M. J. (2014). Pure and zinc doped nano-hydroxyapatite: Synthesis, characterization, antimicrobial and hemolytic studies. *Journal of Crystal Growth, 401,* 474–479. DOI 10.1016/j.jcrysgro.2014.01.062.
42. Tite, T., Popa, A. C., Balescu, L. M., Bogdan, I. M., Pasuk, I. et al. (2018). Cationic substitutions in hydroxyapatite: Current status of the derived biofunctional effects and their in vitro interrogation methods. *Materials, 11(11),* 2081. DOI 10.3390/ma11112081.
43. Ungureanu, D. N., Avram, D., Catangiu, A., Anghelina, F. V., Despa, V. (2015). Characterization of calcium phosphate ceramics obtained by chemical precipitation. *Journal of Optoelectronics and Advanced Materials, 17(7–8),* 1225–1230.
44. Victor, S. P., Paul, W., Vineeth, V. M., Komeri, R., Jayabalan, M. et al. (2016). Neodymium doped hydroxyapatite theranostic nanoplatforms for colon specific drug delivery applications. *Colloids and Surfaces B: Biointerfaces, 145,* 539–547. DOI 10.1016/j.colsurfb.2016.05.067.
45. Webster, T. J., Ergun, C., Doremus, R. H., Bizios, R. (2002). Hydroxylapatite with substituted magnesium, zinc, cadmium, and yttrium. II. Mechanisms of osteoblast adhesion. *Journal of Biomedical Materials Research, 59(2),* 312–317. DOI 10.1002/jbm.1247.
46. Witte, F., Feyerabend, F., Maier, P., Fischer, J., Störmer, M. et al. (2007). Biodegradable magnesium-hydroxyapatite metal matrix composites. *Biomaterials, 28(13),* 2163–2174. DOI 10.1016/j.biomaterials.2006.12.027.
47. Wu, H. C., Wang, T. W., Lin, F. H., Sun, J. S. (2011). Characterization of magnetic hydroxyapatite nanocrystallites and potential application for MRI contrast agent. *Current Nanoscience, 7(6),* 902–907. DOI 10.2174/157341311798220754.
48. Yang, Z., Liu, J., Liu, J., Chen, X., Yan, T. et al. (2021). Investigation on physicochemical properties of graphene oxide/nano-hydroxyapatite composites and its biomedical applications. *Journal of the Australian Ceramic Society, 57(2),* 625–633. DOI 10.1007/s41779-021-00568-3.
49. Zhao, J., Liu, Y., Sun, W. B., Zhang, H. (2011). Amorphous calcium phosphate and its application in dentistry. *Chemistry Central Journal, 5(1),* 1–7. DOI 10.1186/1752-153X-5-40.
50. Zheng, K., Torre, E., Bari, A., Taccardi, N., Cassinelli, C. et al. (2020). Antioxidant mesoporous Ce-doped bioactive glass nanoparticles with anti-inflammatory and pro-osteogenic activities. *Materials Today Bio, 5,* 100041. DOI 10.1016/j.mtbio.2020.100041.